Influence of loading rate on the mechanical performance of metallic glass

Huráková, Mária; Csach, Kornel; Juríková, Alena; Miškuf, Jozef; Demčák, Štefan; Ocelík, Václav; De Hosson, Jeff Th M.

Published in:
Journal of Non-Crystalline Solids

DOI:
10.1016/j.jnoncrysol.2017.05.023

Journal of Non-Crystalline Solids 470 (2017) 160–167

Contents lists available at ScienceDirect

Journal of Non-Crystalline Solids

journal homepage: www.elsevier.com/locate/jnoncrysol

Influence of loading rate on the mechanical performance of metallic glass

Mária Huráková[a,*], Kornel Csach[a], Alena Juríková[a], Jozef Miškuf[a], Štefan Demčák[b], Václav Ocelík[c], Jeff Th.M. De Hosson[c]

[a] Institute of Experimental Physics, Slovak Academy of Sciences, Watsonova 47, 040 01 Košice, Slovakia
[b] Department of Environmental Engineering, Faculty of Civil Engineering, Technical University of Košice, Vysokoškolská 4, 040 01 Košice, Slovakia
[c] Department of Applied Physics, Zernike Institute for Advanced Materials, Faculty of Science and Engineering, University of Groningen, Nijenborgh 4, 9747 AG Groningen, The Netherlands

ARTICLE INFO

Keywords:
Metallic glass
Nanoindentation
Cube corner indenter
Pop-ins
Loading rate
Hardness

ABSTRACT

Amorphous metallic glass $Cu_{47}Ti_{35}Zr_{11}Ni_6Si_1$ was investigated by load-control nanoindentation experiments using the cube corner indenter tip over a wide range of loading rates. The indentation hardness was calculated using different methods either from the loading curves or indent area. Pop-in events were observed on the loading part of the indentation curves mainly at lower rates of loading. Instantaneous plastic deformation decreases with increasing loading rate according to a power law. At high loading rate the instantaneous deformation is suppressed by continuous plastic deformation and no well-developed pop-ins are observed. The morphology of shear bands in the pile-up area of indents showed no correlation with the pop-in event population of the nanoindentation curves and the loading rate.

1. Introduction

Metallic glasses having an amorphous structure show a completely different deformation mechanism in comparison with conventional crystalline materials due to their absence of grain boundaries and lattice dislocations. The conventional theory of lattice dislocations cannot be used for an explanation of plastic deformation of metallic glasses and at the ambient temperature deformation occurs by the formation and localization of shear bands [1–3].

In recent years, the method of nanoindentation has been commonly used to investigate the phenomenon of plastic deformation of metallic glass ribbons at room temperature because of this technique allows to obtain a high resolution in recording load-displacement data [2,4–6].

Spatially and temporally inhomogeneous plastic deformation of metallic glasses is characterized by the creation and propagation of individual shear bands. It turned out that the work softening is closely related to the localization of shear bands but the stress of shear band propagation is less than the stress needed to the initiation of shear bands [7]. Therefore it is possible to observe the serrated flow in metallic glasses which manifests itself as small displacement bursts or load drops during plastic deformation with nanoindentation or in compression experiments [7–9]. In load-displacement indentation curves (*P-h* curves) during load-control nanoindentation experiment discontinuities (pop-ins) can be observed. Discontinuous plastic flow is characterized by repeating the cycles of a sudden stress drop during the nanoindentation experiment with a controlled movement of the indenter into the surface of the material [10]. Wright et al. [11] and Golovin et al. [12] found that the onset of plasticity during nanoindentation of bulk metallic glasses occurs at discrete serrated displacement at the beginning of the *P-h* curve. It has been shown that the nature of pop-ins in *P-h* curve during nanoindentation depends on the composition and the structure of metallic glasses, on the loading rate and the temperature [13–15]. Shear bands in the pile-up area of the indent have been observed in Mg-, Pt-, Pd-, Cu-, Ni- and Fe-based metallic glasses. After nanoindentation of Fe- and Ni-based metallic glasses the relatively small number of shear bands around of indent after nanoindentation was observed. However, the shear bands in the indent area clearly indicate that plastic deformation of metallic glasses is highly localized and inhomogeneous, regardless of the occurrence of pop-ins in *P-h* curve [14,16].

Schuh et al. [2,17–19] described the dependence of deformation of metallic glasses on the loading rate during the nanoindentation experiment. They found that a low loading rate supports the occurrence of pop-in events in *P-h* curves, while high loading rates can partly or completely suppress the formation of pop-ins. The pop-in events in *P-h* curve are magnified with the increasing load or the displacement into surface of material what can be caused by geometry of the indenter tip. Greer et al. [20] noted that the absence of pop-ins at higher loading

* Corresponding author.
E-mail addresses: hurakova@saske.sk (M. Huráková), csach@saske.sk (K. Csach), akasard@saske.sk (A. Juríková), miskuf@saske.sk (J. Miškuf), stefan.demcak@tuke.sk (Š. Demčák), v.ocelik@rug.nl (V. Ocelík).

http://dx.doi.org/10.1016/j.jnoncrysol.2017.05.023
Received 8 March 2017; Received in revised form 10 May 2017; Accepted 15 May 2017
Available online 18 May 2017

rates is only due to a lack of resolution of nanoindentation equipment at low penetration depth. Bei et al. [21] observed that the first pop-in occurred at a load of about 1.2 mN and corresponded to a transition from perfectly elastic to plastic deformation, which is considered as the onset of plastic flow in investigated metallic glasses.

Several indentation studies have pointed out that there is a correlation between the number of slip markers and the number of strain serrations on the *P-h* curve: the higher is the number of shear bands the higher is the number of pop-ins. This might mean that strain serrations can be directly determined by formation of localized macroscopic shearing and each pop-in event that occurs during nanoindentation of metallic glasses corresponds to a single shear event [4,5,11,12,18,22–24].

The understanding the deformation behaviour of metallic glasses can be enhanced through the nanoindentation technique. Remaining questions are how the serrated flow is formed and where the origin of a shear band is, even though it is widely accepted that the flow serration is strongly associated with the shear band creation. In this work we concentrated on the deformation behaviour of Cu-based metallic glass ribbon using nanoindentation over a wide range of loading rates. We focused on the detailed in-depth statistical analysis of the contributions of the instantaneous and continuous displacements at individual pop-in events. Common features of plastic deformation and morphologies of pile-up area of indents occurring at different loading rates were also investigated.

2. Experimental

An amorphous metallic ribbon with the nominal composition of $Cu_{47}Ti_{35}Zr_{11}Ni_6Si_1$ (at%) and with the cross-section of 1.72 mm × 0.02 mm was prepared by rapid melt quenching on a spinning metallic disc. The structure of the ribbon was investigated by X-ray diffraction (XRD) using the Philips X'Pert Pro diffractometer equipped with Cu cathode at operating parameters of 40 kV and 50 mA. Thermal behaviour was examined using of a differential scanning calorimeter, applying the heating rate of 10 °C/min under a nitrogen flow using DSC Q2000-TA Instruments apparatus.

The metallic glass ribbon was studied by means of the nanoindentation technique using the equipment MTS NanoIndenter® XP with cube corner indenter tip. Before nanoindentation test the specimens were mechanically polished to mirror finish and for calibration procedure the fused silica was used. Nanoindentation measurements were performed at room temperature (around 20 °C) in the load rate-control mode up to the maximal load P_{max} = 250 mN. Five loading rates of 0.05, 0.1, 1, 10 and 100 mN·s^{-1} followed by holding for 1 s and then unloading were used and for each measurement up to twenty-five indents were made. High data acquisition rate up to the 25 Hz was chosen for resolving rapid dynamic events. After nanoindentation the morphologies of indent area and shear bands were observed by scanning electron microscope XL30S SEM-FEG.

3. Results and discussion

XRD and DSC analyses confirmed that as-cast amorphous metallic ribbon $Cu_{47}Ti_{35}Zr_{11}Ni_6Si_1$ has an amorphous structure. As Fig. 1a shows XRD pattern of the sample reveals no distinct (crystalline) peaks but only characteristic an amorphous broad maximum centred approximately at 2θ = 42°. DSC scan in Fig. 1b performed at the heating rate of 10 °C/min reveals the midpoint of glass transition at the temperature around of 442.5 °C and the onset temperature of crystallization T_{on} at 452.2 °C.

The load-displacement (*P-h*) curves of the studied alloy during indentation with loading rates d*P*/d*t* ranging from 0.05 to 100 mN·s^{-1} are shown in Fig. 2. The curves were shifted along the displacement axis for a better presentation. The shape of indentation curves is similar for all loading rates applied. Individual pop-ins are more developed at the

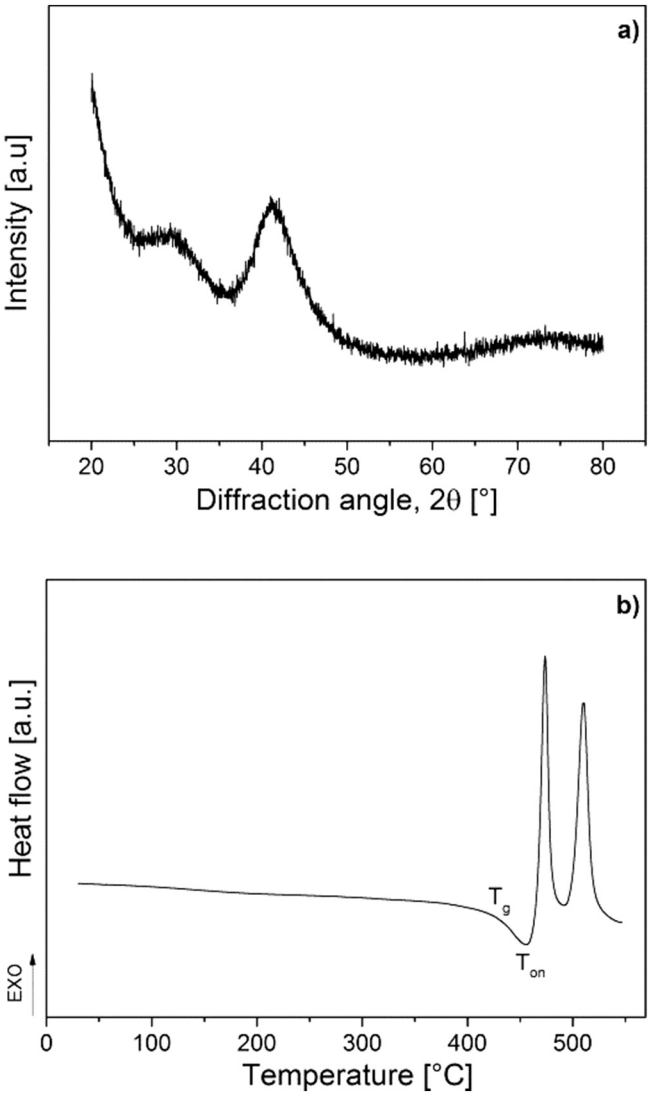

Fig. 1. Typical a) XRD and b) DSC scan of the metallic glass ribbon $Cu_{47}Ti_{35}Zr_{11}Ni_6Si_1$.

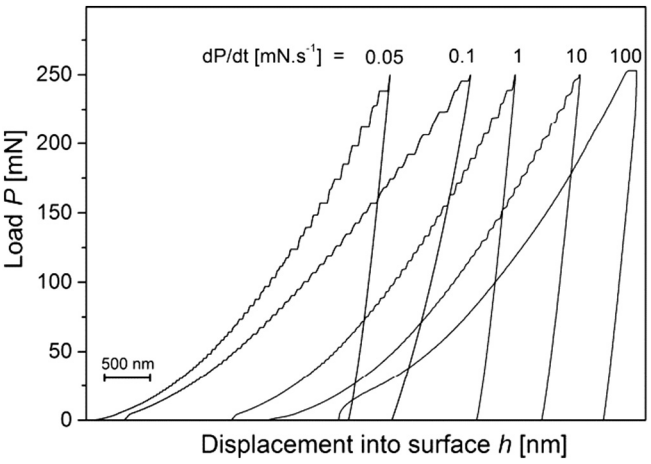

Fig. 2. *P-h* indentation curves for all used loading rates.

lower loading rates (0.05 and 0.1 mN·s^{-1}) and gradually diminish with increasing the loading rate. In *P-h* curves at loading rate of 100 mN·s^{-1} no visible serrated flow was observed.

The hardness of Cu-based amorphous ribbon was estimated by different methods using the measurements of indent area on SEM

pictures or by analyzing of loading curves obtained at nanoindentation with different loading rates.

From morphology of the indent, the area of pile-up around the indent can be determined using Heron's formula for a triangle form of the indent as $S = \sqrt{s(s-a)(a-b)(s-c)}$, where a, b, c are triangle sides and s is a half the perimeter of the triangle $s = (a+b+c)/2$. Then the indentation hardness can be calculated as:

$$H_H = \frac{P_{max}}{S}. \tag{1}$$

The indentation hardness can also be determined by two other methods from *P-h* data obtained during nanoindentation. The first method is based on the work by Oliver and Pharr [25] where the unloading part of a nanoindentation curve can be used for calculation the hardness H_{OP} according to:

$$H_{OP} = \frac{P_{max}}{A_p}, \tag{2}$$

where A_p is projected contact area at loading which is the function of the depth h_c and for cube corner indenter can be calculated as $A_p = 2.6\, h_c^2$ [26]. The depth of the contact indenter with the sample, i.e. the contact depth h_c, is equivalent to the extrapolating depth h_p (determined from the slope of the unloading part of indentation curve) and can be calculated as $h_c = h_{max} - \varepsilon(h_{max} - h_p)$, where ε is geometric factor equal to 0.75 for cube corner indenter tip [26].

The second method for nanoindentation hardness estimation is based on the work by Tuck et al. [27] where the indentation hardness can be calculated from the work of indentation:

$$H_T = \frac{\kappa P_{max}^3}{9 W_{pl}^3}, \tag{3}$$

where κ is a constant equal to 0.04 for cube corner indenter tip. Plastic indentation work W_{pl} can be directly determined through the integral of indentation curves as the difference between total indentation work W_{total} and elastic indentation work W_{el} [27]. Total indentation work W_{total} was determined by integration of nanoindentation curves according to $W_{total} = \int_0^{h_{max}} P(h)dh = W_{pl} + W_{el}$.

The hardness at nanoindentation estimated by different methods is shown in Fig. 3. For each loading rate, approximately ten of *P-h* curves were analyzed. Cu-based amorphous metallic ribbon exhibits the average indentation hardness of 9.11 ± 0.75 GPa using Oliver and Pharr method (Eq. (2)); 9.16 ± 0.89 GPa using Tuck et al. method (Eq.

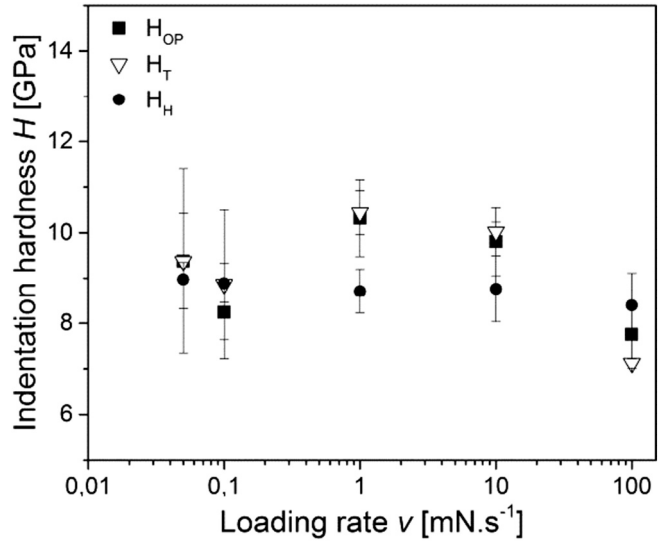

Fig. 3. Dependence of indentation hardness on the loading rate evaluated by different methods (H_{OP} - Oliver Pharr method [25], H_T - according to Tuck [27] and H_H - from indent area).

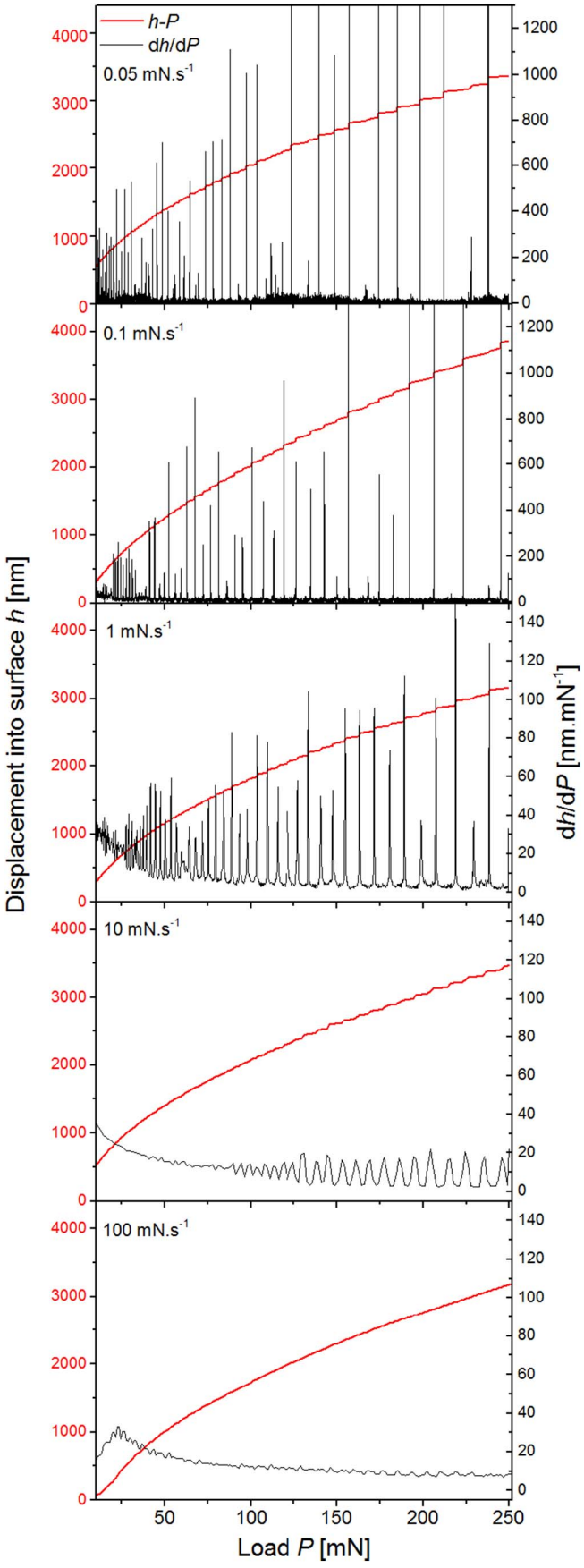

Fig. 4. Dependencies of displacement into surface on load (*h-P* curve) and their derivatives with respect to the load (d*h*/d*P*) for indicated loading rates. Note increasing dh/dP range with decreasing loading rate.

(3)) and 8.75 ± 0.55 GPa using indent area measurements. Each method applied for the calculation of the indentation hardness is in good agreement among each other. No systematic difference was observed for hardness estimated by different methods.

The contributions of the pop-ins to the total plastic deformation in metallic glasses are very useful parameters in understanding the mechanical performance [11,12,19,20,25,28]. The dependencies of displacement into surface on load (*h*-*P* curve) and their first order numeric derivatives without smoothing with respect to the load (d*h*/d*P*) for all loading rates are displayed in Fig. 4. At the pop-in event the displacement curve reveals a step whereas the load remains constant, so the sharp peak on the derivative curve is present. We suppose that the background noise is caused not only by fluctuation of experimental conditions but also by small shear displacements in deformed pile-up area around the indent. As the loading rate increases, the threshold value of the load for the generation of the first significant pop-in increases up to the value of 80 mN at loading rate of 10 mN·s^{-1}. At a lower load in the beginning stage of indentation the load difference between peaks is low and continuously increases with increasing load. With increasing loading rate, the sharp peaks become wider and their height decreases. The derivative curves enable also a better distinction in the number of pop-ins. At lower loading rates the total number of sharp peaks was found to be about 25–35. As the loading rate increases to 10 mN·s^{-1} the number of peaks decreases to about 20–25 what is caused mainly by vanishing of the peaks at lower loads. Moreover, the peaks at higher loads show up more homogeneously in form and period. For the highest loading rate of 100 mN·s^{-1} pop-ins vanish completely and only small undulations on the derivative curve are detected.

There are various explanations about the absence of pop-in events in nanoindentation curves at higher loading rates. Schuh et al. [19] found that significant pop-in events are present only at strain rates below about 1 to 10 s^{-1}. According to Greer et al. [20] it can be caused by the instrumental blurring at higher loading rates.

Another way for quantitative description of serrated plastic deformation during nanoindentation is based on the concept of the discrete plasticity ratio [17,18,24,29]. The concept of this parameter is schematically illustrated in Fig. 5. During nanoindentation the total displacement is a superposition of three components: an instantaneous part of the plastic deformation (Δh_{ID}), a continuous part of the plastic deformation (Δh_{CD}) and an elastic part of the deformation (Δh_{el}). It is expected that during unloading the elastic deformation will be fully recovered and the portion of plastic deformation (Δh_{pl}) is simply given by the sum of Δh_{ID} and Δh_{CD}. Thus, the contribution of instantaneous plasticity to the total plasticity (named discrete plasticity ratio) is given as $\Delta h_{ID}/\Delta h_{pl}$. This parameter indicates the fraction of plastic deformation that can be attributed to the discrete pop-in event. For perfectly homogeneous flow the index of the serration flow equals to zero and for perfectly instantaneous deformation the value of unity is reached [1].

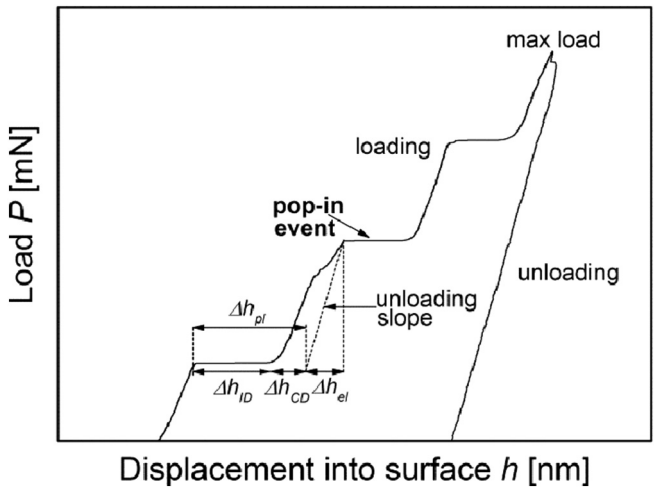

Fig. 5. The scheme of estimation the plastic and the elastic component of the deformation at a pop-in event [30,31].

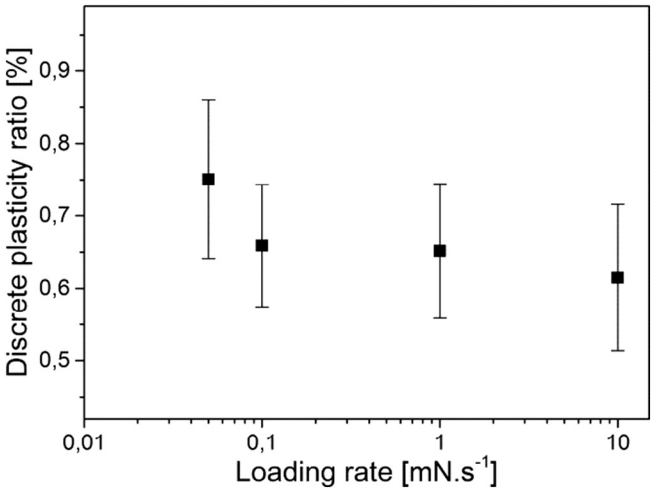

Fig. 6. Discrete plasticity ratio as a function of the loading rate.

We studied the individual components of displacement near a pop-in on the loading curves. The well-developed pop-ins with instantaneous deformation jump of about 10 nm and more were analyzed (about 150–180 individual pop-in events for each loading rate). For loading rate of 100 mN·s^{-1} the pop-ins were not developed to the form suitable for regular quantification of individual pop-ins.

In Fig. 6 the discrete plasticity ratio $\Delta h_{ID}/\Delta h_{pl}$ is plotted as a function of the loading rate. The discrete plasticity ratio parameter varies from 0.75 to 0.62. The tendency to the decrease of this parameter with the increase of the loading rate can be supposed. However, the extrapolation of this dependence to the loading rate of 100 mN·s^{-1} does not reach the value of zero as expected in the case of vanishing pop-in events at perfectly homogeneous deformation at the highest loading rate. This is due to the fact that the values of discrete plasticity ratio in Fig. 6 are averaged from measured well-developed pop-ins while the pop-ins with very small step are not taken into account. Although the deformation components were analyzed for well-developed pop-ins, their properties can be extended by an extrapolation to the small pop-ins.

Load dependency of individual depth increment components (h_{ID}, h_{CD}) at which pop-ins were analyzed are shown in Fig. 7. As the loading rate increases, the threshold value of load at which the first well-developed pop-in is propagated, increases. For lower loading rates the first pop-in events are present on loading part of indentation curve from its beginning and the pop-ins are well developed at loading of about 25 mN, whereas at loading rate of 10 mN·s^{-1} the pop-ins were present at the loads higher than 110 mN.

As can be seen in Fig. 7, the individual components of deformation (points) are accumulated along lines and therefore they were linearly fitted with the results summarized in Table 1. We can conclude that the contribution of the continuous deformation h_{CD} to the total deformation at pop-in events is always smaller than the contribution of the instantaneous deformation and does not follow a systematic dependence on the loading rate. However, the contribution of the instantaneous deformation h_{ID} at individual pop-in event depends on the load at which the pop-ins occur. The slope of linear fit can be assigned as the instantaneous deformation (ID) sensitivity coefficient. It is shown in Table 1 that this coefficient varies from 0.26 for loading rate of 0.05 mN·s^{-1} to the value of 0.12 for 10 mN·s^{-1} loading rate with a clear decreasing tendency with increasing loading rate. Extrapolation of instantaneous deformation h_{ID} for zero loads gives the value of about 18 ± 2 nm independently on the loading rate. This value can be assumed as a minimal depth increment at instantaneous deformation

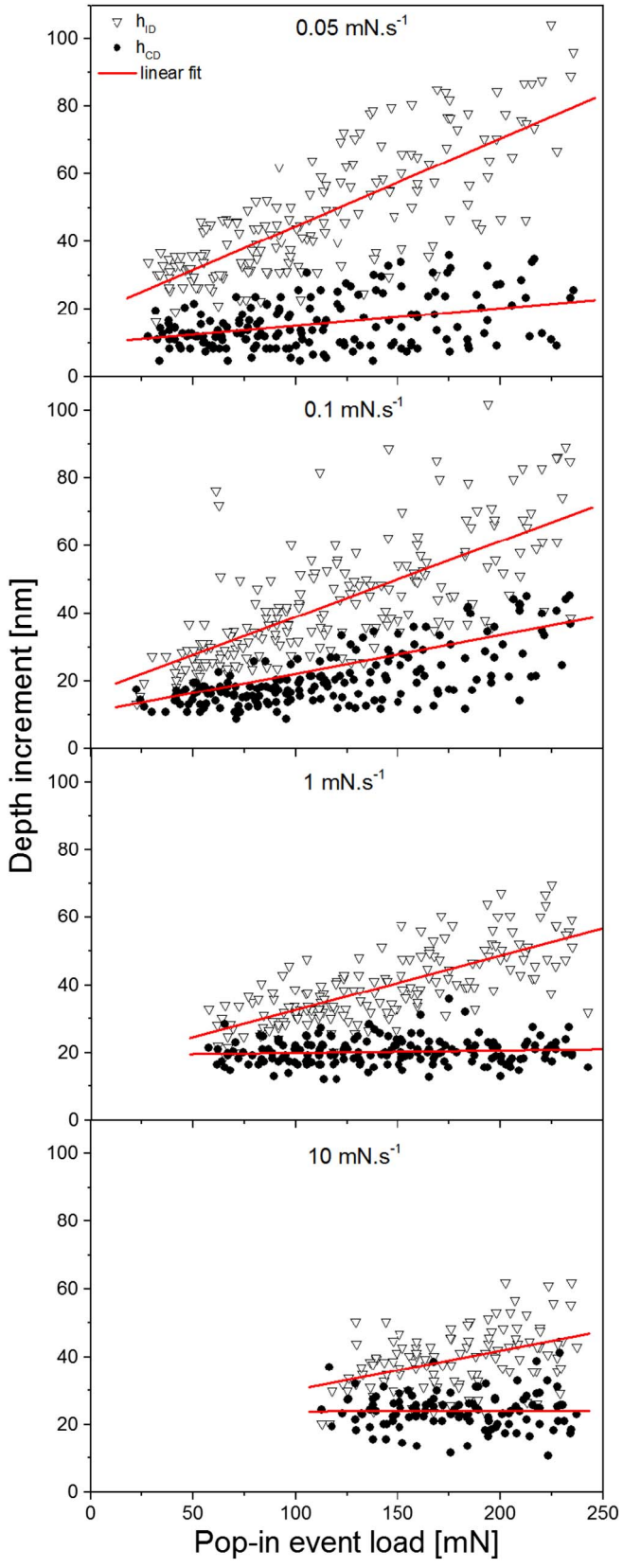

Fig. 7. Individual components of the deformation as a function of pop-in event load.

for one pop-in event. Regarding the continuous deformation h_{CD}, it shows different behaviour. The continuous displacement corresponding to a pop-in event reaches the values of 5–40 nm and no substantial dependency on the loading rate or the load was observed.

Table 1
Deformation sensitivity coefficients for used loading rates.

Loading rate [mN·s^{-1}]	Sensitivity coefficient [nm·mN^{-1}] of individual deformation components	
	h_{ID}	h_{CD}
0.05	0.26 ± 0.02	0.05 ± 0.01
0.1	0.22 ± 0.02	0.10 ± 0.01
1	0.16 ± 0.01	0.01 ± 0.01
10	0.12 ± 0.02	0.001 ± 0.02

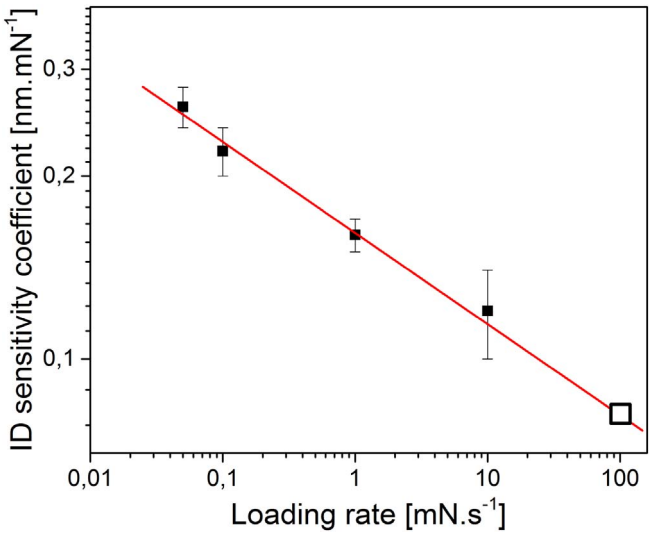

Fig. 8. Dependence of instantaneous deformation sensitivity coefficient on the applied loading rate. The empty square symbol shows the extrapolated value for loading rate of 100 mN·s^{-1}.

The dependence of the instantaneous deformation sensitivity on the applied loading rate v was fitted with a power law according to: $h_{ID} = Av^B$ as shown in Fig. 8. The least square fit gave the values $A = 0.16 \pm 0.01$ and $B = -0.15 \pm 0.01$ with high correlation coefficient 0.9824. The extrapolation of this dependence to the loading rate of 100 mN·s^{-1} gives the ID sensitivity coefficient of about 0.08. Although the fit in Fig. 8 was made through only four points, we assume that it is sufficient for determination the dependence formula and for the estimation of instantaneous deformation sensitivity coefficient by extrapolation to higher loading rates.

Assuming that this law is valid over the whole interval of loading rates we can predict the expected instantaneous displacements for the loading rate of 100 mN·s^{-1} using the relation: $h_{ID} = 18 + 0.08P$. From that h_{ID} reaches values in the range from 18 to 38 nm as the load varies from 0 to 250 mN. This range corresponds to the values for continuous deformation contribution h_{CD} (5–40 nm). Coincidence of intervals of h_{ID} and h_{CD} values can be assigned as a reason for the vanishing of the serrated flow manifestations during loading at nanoindentation at higher rates. In addition, it can also explain the increase in the threshold load for formation of the first well-developed pop-in with increasing the loading rate. The physical nature of these dependences needs further investigations.

After nanoindentation the morphology of the area of indents was inspected in detail with scanning electron microscopy. Fig. 9 illustrates the plastic flow around cube corner indents on the surface of Cu-based metallic glass for all loading rates used (sorted from the lowest to the highest). The indent area and the deformed volume in pile-up area are relatively large due to the cube corner indenter tip form and maximal used loading of 250 mN. The size of the indent and the form of plastic deformed area seem to be preserved for all applied loading rates. The pile-up area of indents shows a plate-like morphology. Details in Fig. 10

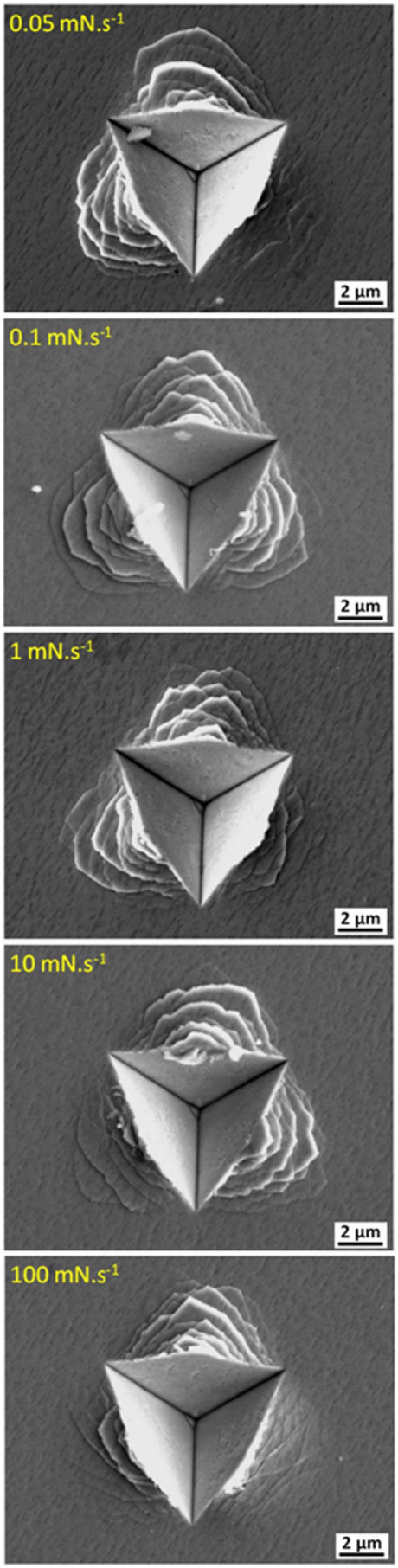

Fig. 9. Morphology of indents for indicated loading rates.

demonstrate the well distinguished plates in pile-up area visible for the samples tilted by angle about 70°. The number of polygonal plates decreases from the value of about 30 for the lowest loading rate to the value of about 25 for the highest loading rate.

The observation of morphology of indent area reveals the presence of dominant shear band system connected with the plate formation. Whereas the form of loading curves changes from stepwise to the smooth as the loading rate increases, the morphology of deformed indent area including the height of the pile-up is unchanged (Fig. 10). The number of well-developed pop-ins on the loading curves at low loading rates approximately corresponds to the number of plates in the final pile-up area observed after indentation event.

High coefficient of the discrete plasticity ratio observed at a loading rate of 0.05 $mN{\cdot}s^{-1}$ shows that about 75% of total plastic deformation is connected with pop-in event mechanism. In this case the presence of the plate-like form of pile-up area around the indent reflects the stepwise plastic deformation behaviour. As the loading rate increases, the portion of instantaneous plastic deformation determined by discrete plasticity ratio concept decreases, and at loading rate of 100 $mN{\cdot}s^{-1}$ the pop-ins vanish. On contrary, the number of plates in the pile-up area changes only slightly. This should be discussed in detail. The plastic deformation in amorphous alloys occurs via creation and propagation of shear bands [11,29,32,33]. It is suggested that at some conditions the plastic deformation is moderated by stepwise nature of shear front propagation [2,14,34]. The generation of secondary shear bands near the existing shear band is affected by structural relaxation of amorphous structure in areas around the existing shear band due to the local heating [35]. We suppose that the existence of minimal instantaneous deformation value h_{ID} is connected with the structural relaxation in layers along shear bands. The shear bands and corresponding relaxed zones are planar. The new shear bands are created in the area outside the affected zone. So the plate-like morphology is formed in both stepwise and continuous deformation manner. Deformation by progressive propagation of shear bands is equivalent to instantaneous deformation at pile-up and the resulting morphology of shear bands pattern around indent shows a similar shape.

Figs. 4 and 8 point out that the sensitivity of pop-in events on the loading is lowered with increasing loading rate. We suppose that structural relaxations occur during plastic deformation in pile-up area. If the loading rate at nanoindentation is low, the high accumulated elastic energy is released in a pile-up event. Due to the structural relaxation the next principal shear band is created in the unaffected region after as enough elastic energy is accumulated. If the loading rate at nanoindentation is high, the structural relaxation in the regions near shear bands is not completed. The increased stress causes the shearing along properly oriented shear bands in the region softened by inhomogeneous plastic deformation. However, for the shear band propagation in the softened regions the lower stress is sufficient and the deformation events occur preferably by continuous deformation or by series of small instantaneous deformations.

4. Conclusion

Nanoindentation experiments of the amorphous metallic ribbon $Cu_{47}Ti_{35}Zr_{11}Ni_6Si_1$ with cube corner indenter tip have revealed the presence of many pop-in events in the loading part of indentation curves at loading rates up to 10 $mN{\cdot}s^{-1}$. It has been found that the pop-ins are influenced by the indentation depth and the loading rate. With decreasing the loading rates the pop-in events are more developed. It is important to note that no simple correlation between the presence of pop-ins and the shear band morphology of the indent region was observed. At low loading rates the plate-like morphology of pile up areas is created by one or small numbers of events with higher deformations, whereas at higher deformation rates the plate-like structure is created via successive small shearing along properly oriented shear bands. Hardness estimated by several methods takes

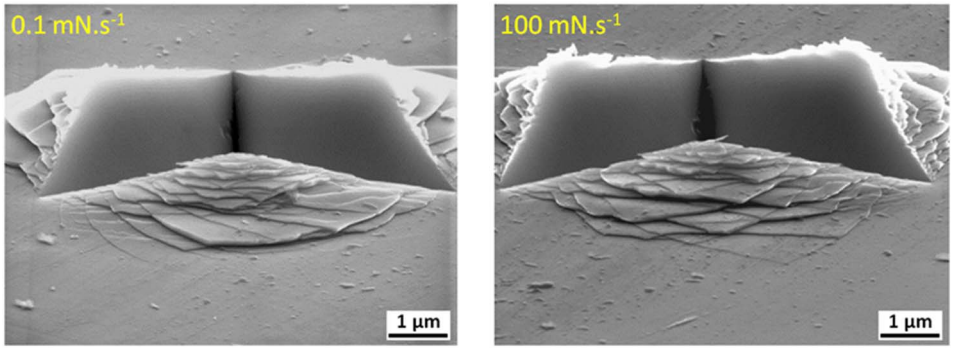

Fig. 10. Morphology of pile-up area around the indent for indicated loading rates. Sample surface normal tilted 70° towards electron beam.

similar values for all loading rates.

It has been revealed that the instantaneous deformation corresponding to a pop-in event during nanoindentation depends on the load whereas the continuous plastic deformation reaches the values of 5 to 40 nm without a simple dependence on either the load or loading rate. We have found that the minimal value of instantaneous displacement of 18 nm exists and does not depend on the loading rate. As the loading rate increases, the sensitivity of instantaneous deformation to the load decreases according to a power law behaviour. By extrapolation of this dependence the expected values for instantaneous deformation at the loading rate of 100 $mN{\cdot}s^{-1}$ were estimated in the range of 18 to 38 nm. At this loading rate the values of instantaneous and continuous deformation steps are comparable and therefore almost no well-developed pop-ins are observed at high loading rates.

Acknowledgment

This work was supported by Slovak Academy of Sciences - grant VEGA 2/0045/14.

References

[1] A.S. Argon, J. Megusar, N.J. Grant, Shear band induced dilations in metallic glasses, Scr. Metall. 19 (1985) 591–596, http://dx.doi.org/10.1016/0036-9748(85)90343-6.
[2] C.A. Schuh, T.G. Nieh, A nanoindentation study of serrated flow in bulk metallic glasses, Acta Mater. 51 (2003) 87–99, http://dx.doi.org/10.1016/S1359-6454(02)00303-8.
[3] T.C. Hufnagel, C.A. Schuh, A. C., M.L. Falk, Deformation of metallic glasses: Recent developments in theory, simulations, and experiments, Acta Mater. 109 (2016) 375–393, http://dx.doi.org/10.1016/j.actamat.2016.01.049.
[4] F. Xu, Z.L. Long, X.H. Deng, P. Zhang, Loading rate sensitivity of nanoindentation creep behavior in a Fe-based bulk metallic glass, Trans. Nonferrous Metals Soc. China 23 (2013) 1646–1651, http://dx.doi.org/10.1016/S1003-6326(13)62643-6.
[5] R. Maaß, D. Klaumünzer, J.F. Löffler, Propagation dynamics of individual shear bands during inhomogeneous flow in a Zr-based bulk metallic glass, Acta Mater. 59 (2011) 3205–3213, http://dx.doi.org/10.1016/j.actamat.2011.01.060.
[6] B.A. Sun, S. Pauly, J. Tan, M. Stoica, W.H. Wang, U. Kühn, J. Eckert, Serrated flow and stick–slip deformation dynamics in the presence of shear-band interactions for a Zr-based metallic glass, Acta Mater. 60 (2012) 4160–4171, http://dx.doi.org/10.1016/j.actamat.2012.04.013.
[7] H. Kimura, T. Masumoto, A model of the mechanics of serrated flow in an amorphous alloy, Acta Metall. 31 (2) (1983) 231–240, http://dx.doi.org/10.1016/0001-6160(83)90100-1.
[8] B. Moser, J. Kuebler, H. Meinhard, W. Muster, J. Michler, Observation of instabilities during plastic deformation by in-situ SEM indentation experiments, Adv. Eng. Mater. 7 (5) (2005) 388–392, http://dx.doi.org/10.1002/adem.200500049.
[9] B. Moser, J.F. Löffler, J. Michler, Discrete deformation in amorphous metals: an in situ SEM indentation study, Philos. Mag. 86 (2006) 5715–5728, http://dx.doi.org/10.1080/14786430600627301.
[10] H.S. Chen, Plastic flow in metallic glasses under compression, Scr. Metall. 7 (1973) 931–935, http://dx.doi.org/10.1016/0036-9748(73)90143-9.
[11] W.J. Wright, R. Saha, W.D. Nix, Deformation mechanisms of $Zr_{40}Ti_{14}Ni_{10}Cu_{12}Be_{24}$ bulk metallic glass, Mater. Trans. 42 (2001) 642–649, http://dx.doi.org/10.2320/matertrans.42.642.
[12] Y.I. Golovin, V.I. Ivolgin, V.A. Khonik, K. Kitagawa, A.I. Tyurin, Serrated plastic flow during nanoindentation of a bulk metallic glass, Scr. Mater. 45 (2001) 947–952, http://dx.doi.org/10.1016/S1359-6462(01)01116-2.
[13] M. Zhang, Y.J. Wang, L.H. Dai, Understanding the serrated flow and Johari-Goldstein relaxation of metallic glasses, J. Non-Cryst. Solids 444 (2016) 23–30, http://dx.doi.org/10.1016/j.jnoncrysol.2016.04.036.
[14] R. Limbach, K. Kosiba, S. Pauly, U. Kühn, L. Wondraczek, Serrated flow of CuZr-based bulk metallic glasses probed by nanoindentation: role of the activation barrier, size and distribution of shear transformation zones, J. Non-Cryst. Solids 459 (2017) 130–141, http://dx.doi.org/10.1016/j.jnoncrysol.2017.01.015.
[15] M. Huráková, K. Csach, A. Juríková, J. Miškuf, Š. Demčák, V. Ocelík, J.Th.M. De Hosson, Serrated plastic flow of various metallic glasses during nanoindentation, Defect and Diffusion Forum, 368 2016, pp. 3–6, , http://dx.doi.org/10.4028/www.scientific.net/DDF.368.3.
[16] W.H. Li, B.C. Wei, T.H. Zhang, D.M. Xing, L.C. Zhang, Y.R. Wang, Study of serrated flow and plastic deformation in metallic glasses through instrumented indentation, Intermetallics 15 (2007) 706–710, http://dx.doi.org/10.1016/j.intermet.2006.10.010.
[17] C.A. Schuh, T.G. Nieh, A survey of instrumented indentation studies on metallic glasses, J. Mater. Res. 19 (2004) 46–57, http://dx.doi.org/10.1557/jmr.2004.19.1.46.
[18] C.A. Schuh, A.L. Lund, T.G. Nieh, New regime of homogeneous flow in the deformation map of metallic glasses: elevated temperature nanoindentation experiments and mechanistic modelling, Acta Mater. 52 (2004) 5879–5891, http://dx.doi.org/10.1016/j.actamat.2004.09.005.
[19] C.A. Schuh, T.G. Nieh, Y. Kawamura, Rate dependence of serrated flow during nanoindentation of a bulk metallic glass, J. Mater. Res. 17 (2002) 1651–1654, http://dx.doi.org/10.1557/JMR.2002.0243.
[20] A.L. Greer, A. Castellero, S.V. Madge, I.T. Walker, J.R. Wilde, Nanoindentation studies of shear banding in fully amorphous and partially devitrified metallic alloys, Mater. Sci. Eng. A 375–377 (2004) 1182–1185, http://dx.doi.org/10.1016/j.msea.2003.10.032.
[21] H. Bei, Z.P. Lu, E.P. George, Theoretical strength and the onset of plasticity in bulk metallic glasses investigated by nanoindentation with a spherical indenter, Phys. Rev. Lett. 93 (2004) 125504, http://dx.doi.org/10.1103/PhysRevLett.93.125504.
[22] H. Bei, S. Xie, E.P. George, Softening caused by profuse shear banding in a bulk metallic glass, Phys. Rev. Lett. 96 (2006) 105503, http://dx.doi.org/10.1103/PhysRevLett.96.105503.
[23] A. Bhattacharyya, G. Singh, K.E. Prasad, R. Narasimhan, U. Ramamurty, On the strain rate sensitivity of plastic flow in metallic glasses, Mater. Sci. Eng. A 625 (2015) 245–251, http://dx.doi.org/10.1016/j.msea.2014.12.004.
[24] G. Liao, Z. Long, M. Zhao, M. Zhong, W. Liu, W. Chai, Serrated flow behavior in a Pd-based bulk metallic glass under nanoindentation, J. Non-Cryst. Solids 460 (2017) 47–53, http://dx.doi.org/10.1016/j.jnoncrysol.2017.01.010.
[25] W.C. Oliver, G.M. Pharr, Measurement of hardness and elastic modulus by instrumented indentation: advances in understanding and refinements to methodology, J. Mater. Res. 19 (2004) 3–20, http://dx.doi.org/10.1557/jmr.2004.19.1.3.
[26] A.C. Fischer-Cripps, Nanoindentation (Mechanical Engineering Series), Springer, USA, 2004, p. 263 (ISBN: 0-387-22045-3).
[27] J.R. Tuck, A.M. Korsunsky, S.J. Bull, R.I. Davidson, On the application of the work-of-indentation approach to depth-sensing indentation experiments in coated systems, Surf. Coat. Technol. 137 (2001) 217–224, http://dx.doi.org/10.1016/S0257-8972(00)01063-X.
[28] A.L. Greer, I.T. Walker, Transformations in primary crystallites in (Fe,Ni)-based metallic glasses, Mater. Sci. Forum 386–388 (2002) 77–88, http://dx.doi.org/10.4028/www.scientific.net/MSF.386-388.77.
[29] T. Mukai, T.G. Nieh, Y. Kawamura, A. Inoue, K. Higashi, Dynamic response of a Pd40Ni40P20 bulk metallic glass in tension, Scr. Mater. 46 (2002) 43–47, http://dx.doi.org/10.1016/S1359-6462(01)01193-9.
[30] M. Huráková, K. Csach, A. Juríková, J. Miškuf, Š. Demčák, V. Ocelík, J.Th.M. De Hosson, Nanoindentation study of the influence of the loading rate on the deformation of metallic glasses, Key Eng. Mater. 662 (2015) 23–26, http://dx.doi.org/10.4028/www.scientific.net/KEM.662.23.
[31] M. Huráková, K. Csach, A. Juríková, J. Miškuf, Š. Demčák, V. Ocelík, J.Th.M. De Hosson, Discontinuities of plastic deformation in metallic glasses with different glass forming ability, Phys. Procedia 75 (2015) 1265–1270, http://dx.doi.org/10.1016/j.phpro.2015.12.140.
[32] V. Ocelik, K. Csach, A. Kasardova, J. Miskuf, H.P. Svec, K. Kristiakova, I. Matko, Activation energy distribution in nanocrystallization kinetics of amorphous $Fe_{73.5}Cu_1Nb_3Si_{13.5}B_9$ alloy, Scr. Mater. 35 (1996) 1301–1306, http://dx.doi.org/10.

1016/1359-6462(96)00307-7.
[33] V. Ocelik, P. Diko, V. Hajko, J. Miskuf, P. Duhaj, Fracture-toughness of some metallic glasses, J. Mater. Sci. 22 (1987) 2305–2308, http://dx.doi.org/10.1007/BF01082108.
[34] J.W. Qiao, H.L. Jia, Y. Zhang, P.K. Liaw, L.F. Li, Multi-step shear banding for bulk metallic glasses at ambient and cryogenic temperatures, Mater. Chem. Phys. 136 (2012) 75–79, http://dx.doi.org/10.1016/j.matchemphys.2012.06.033.
[35] D.T.A. Matthews, V. Ocelik, P.M. Bronsveld, J.Th.M. De Hosson, An electron microscopy appraisal of tensile fracture in metallic glasses, Acta Mater. 56 (2008) 1762–1773, http://dx.doi.org/10.1016/j.actamat.2007.12.029.